Molecular Therapy
Methods & Clinical Development
Original Article

Polo-like kinase inhibitors increase AAV production by halting cell cycle progression

Kaylin Fisher,[1] Francis Grafton,[1] Francesca Ispaso,[1] Joshua Tworig,[1] Rupert Derler,[2] Florian Sonntag,[2] Markus Hörer,[2] Andreas Schulze,[2] Christopher A. Reid,[1] and Mohammad A. Mandegar[1]

[1]Ascend Advanced Therapies CA Inc, Alameda, CA 94501, USA; [2]Ascend Advanced Therapies GmbH, 82152 Planegg, Germany

Recombinant adeno-associated viruses (rAAVs) are commonly used in gene therapy for preclinical research and therapeutic applications. Despite the clinical efficacy of rAAVs, their manufacturing involves challenges in productivity and quality, leading to limited availability. In this study, we aimed to identify compounds that increase the capacity of cells to produce AAV9 with a high-throughput small-molecule screening strategy. With the Arrayed Targeted Library for AAV Screening platform, we screened a library of 3,300 small molecules and identified several targets, including cell cycle modulators, G protein-coupled receptor modulators, histone deacetylate inhibitors, Janus kinase inhibitors, and metabolic modulators. Most notably, we identified Polo-like kinase isoform 1 (PLK1) inhibitors as enhancers of adeno-associated virus (AAV) production. Inhibiting PLK1 with HMN-214 increased AAV production, which was largely consistent across HEK293 cell lines, vector payloads, and capsid serotypes. Using cell cycle and RNA-sequencing analysis, we showed that PLK1 inhibition halts cells in the G2/M phase and blocks their exit from the M to G1 phase. These findings support that inhibiting PLK1 may enhance AAV production and could be used to develop more cost-effective methods to manufacture AAV for gene therapies.

INTRODUCTION

Adeno-associated viruses (AAVs) are commonly used in gene therapy for preclinical research and therapeutic applications.[1,2] These nonpathogenic parvoviruses are approximately 4.7 kb, have a well-established safety profile, and are nonpathogenic and non-integrating. AAV capsids can also be engineered to increase vector tropism, which allows AAVs to more efficiently deliver to the desired tissue type, reduce the host immune response, and de-target from non-desired tissues for better safety.[3] These vectors are already considered mostly safe and well-tolerated, because more than 3,000 patients have been given AAV gene therapies.[4] Also, as of 2024, eight AAV gene therapies have been approved by either the Food and Drug Administration or the European Medicines Agency (Glybera was first approved for lipoprotein lipase deficiency and then withdrawn due to commercial considerations).[5,6] In addition, more than 700 programs are in development in various stages from preclinical to late-stage clinical trials.[4,6–10]

These AAV-based gene therapy clinical trials have predominantly targeted mid-size, rare monogenic indications.[11] However, this focus is expanding as several preclinical programs explore more common indications and refine methods of delivering pathway-modifying payloads.[6,11] These common indications include diabetes,[12] hypertension,[13] Alzheimer's disease,[14,15] and heart failure.[16–19] However, the vector demand and high costs of these treatments, especially for systemically delivered therapies, hinder widespread adoption of these lifesaving medicines.[6,11,20]

Challenges preventing widespread use of AAV-based therapies relates to constraints with their manufacturing.[20] These constraints include low volumetric yields[21] and high batch-to-batch variability.[22] They also include poor quality due to low full-to-empty capsid ratios and packaging of undesired, potentially harmful DNA sequences.[23,24] To improve AAV manufacturing, most efforts have focused on design of experiment (DoE) strategies, including the composition of cell culture media, the density of host cells, transfection reagents, and plasmid ratios and sizes.[25–27] Although DoE studies are needed to optimize AAV bioproduction, their effectiveness is constrained within the boundaries of an existing manufacturing platform, and they typically lead to only marginal improvements. Therefore, DoE studies alone may not be enough to drive enhancements in AAV production.[6] As a result, improvement efforts have now expanded from DoE studies to include (1) generating clonal[28] and stable producer cell lines[29,30] (2) using the self-attenuating adenovirus (tetracycline-enabled self-silencing adenovirus [TESSA]) platform,[31] (3) supplementing with microtubule and histone deacetylase inhibitors,[32] (4) modulating MAPK signaling with miR-431 and miR-636,[33] (5) activating SKA2 and ITPRIP with CRISPR,[34] and (6) knocking out endoplasmic reticulum-Golgi membrane components (TMED2, TMED10, MON2).[35]

In this study, we aimed to identify small molecules that enhanced rAAV production for research, preclinical, and ultimately clinical applications. To identify enhancers that increased the AAV production capacity of cells, we completed a high-throughput small-molecule screen of bioactive compounds with our Arrayed Targeted Library for AAV Screening (ATLAS) platform.[36] We then confirmed the

Received 13 November 2024; accepted 14 January 2025;
https://doi.org/10.1016/j.omtm.2025.101412.

Correspondence: Mohammad A. Mandegar, Ascend Advanced Therapies CA Inc, Alameda, CA 94501, USA.
E-mail: mandegar@gmail.com

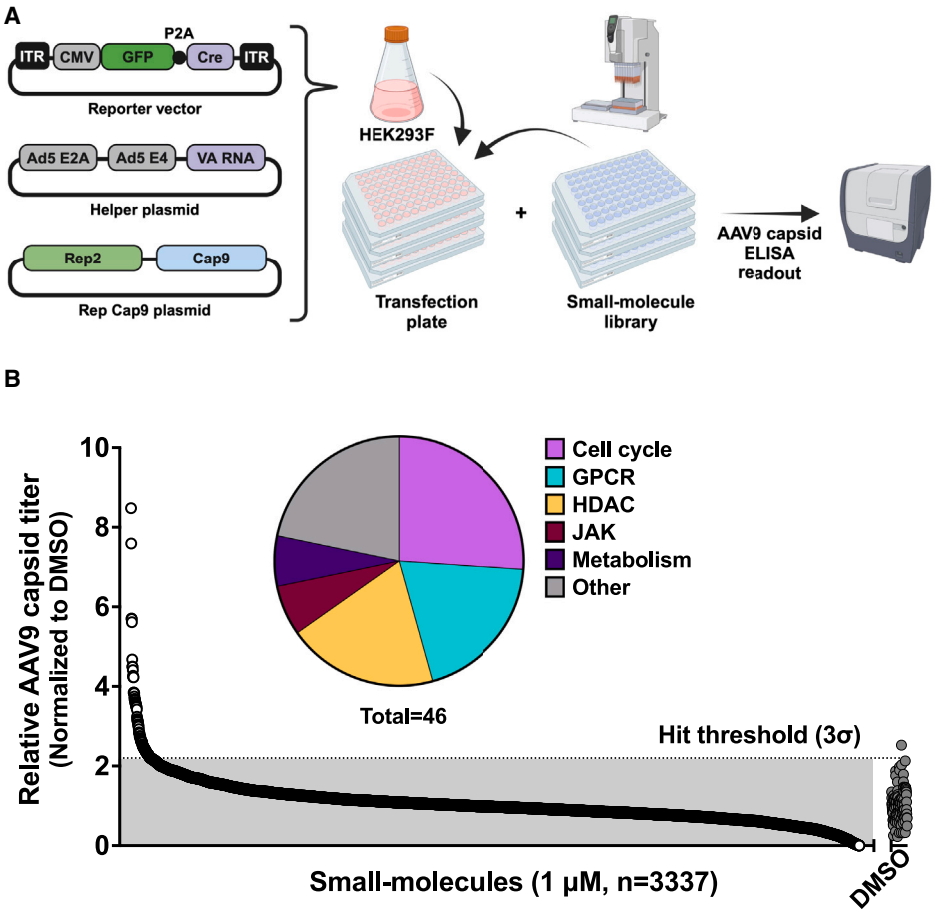

(legend on next page)

effects of the identified compounds on AAV production in multiple validation studies.

RESULTS

A high-throughput screening platform to identify enhancers of AAV production

To identify candidate targets and pathways that improve AAV production, we developed ATLAS, a high-throughput screening platform.[36] This platform is modality-agnostic and amenable to gain-of-function and loss-of-function screens. Before the screen, we optimized the cell-seeding density and transfection conditions in adherent human embryonic kidney (HEK) cells (Figure S1A).

Next, we developed a cell-based functional titer assay to enable high-throughput measures of functional AAV particles in microwell plates. To overcome the low efficiency of *in vitro* AAV9 transduction in cells,[37] we developed a reporter cell line that contains a flipped mCherry-P2A-NanoLuciferase (NLuc) flanked by *loxP* sites. When these reporter cells are introduced to a GFP-Cre-expressing AAV vector containing an inverted terminal repeat (ITR), the mCherry-P2A-NLuc cassette is flipped to allow detection of both the mCherry and NLuc signals (Figures S1B–S1D).

To rapidly validate primary hits in suspension HEK293 cells, we also optimized AAV production using a 96-well suspension format (Figures S1E and S1F). With these conditions (detailed in the materials and methods), we obtained similar yields of AAV9 vector genome in 96-well, 6-well, and 125-mL shake flask suspension vessel formats. Higher vector genome titers per cell were obtained in the Ambr15 microbioreactor and adherent formats (Figure S1G).

Compound screen identifies cell cycle modulators as putative enhancers of AAV9 production

To identify compounds that enhance AAV9 production, we completed a high-throughput screen of a library of approximately 3,300 bioactive small molecules. For this screen, we triple-transfected HEK293F cells with a Rep Cap9 plasmid, Helper plasmid, and ITR-containing reporter vector. Then we seeded the transfected cells onto 96-well plates and performed an arrayed screen with the bioactive small-molecule library at a 1 μM dose (Figure 1A). Then we determined the capsid titer with AAV9 capsid ELISA (enzyme-linked immunosorbent assay). We normalized the results from the primary screen to the dimethyl sulfoxide (DMSO) mean across all plates and ordered them by rank (Figure 1B). The top-performing compounds that increased AAV9 capsid titer 3σ above the DMSO mean were clustered into five pathways or target classes: cell cycle modulators, G protein-coupled receptor (GPCR) modulators, histone deacetylase (HDAC) inhibitors, Janus kinase (JAK) inhibitors, and metabolic targets. All 46 compounds identified in the primary screen are summarized in Table S1.

Polo-like kinase and microtubule inhibitors increase AAV9 capsid titer and functional titer in HEK293 cells

To confirm the top hits from the primary screen, we treated adherent HEK293 cells with four doses of compounds identified from the primary screen and measured the capsid titer with an AAV9-capsid ELISA. We found that a Polo-like kinase 1 (PLK1) inhibitor (HMN-214) and microtubule inhibitors (combretastatin A4, vindesine sulfate, ansamitocin p-3, and monomethyl auristatin E [MMAE]) increased the titer of AAV9 capsids by more than 1.6-fold vs. the DMSO control (Figure 1C). We also measured the relative AAV9 functional titer using a cell-based assay (described in Figures S1B–S1D) and plotted these data against the capsid titer (Figure 1D). The top two performing compounds that increased both capsid titer and functional titer were HMN-214 and Combretastatin A4. To test if co-administration of HMN-214 and microtubule inhibitors further boost AAV9 production, two microtubule inhibitors (Combretastatin A4 and MMEA) were first tested as a single agent in suspension HEK293 cells. Both Combretastatin A4 and MMEA showed a dose-dependent increase in AAV9 production (Figure S2A). However, combination of Combretastatin A4 and HMN-214 did not show an increase in AAV9 production (Figure S2B).

Given that microtubule inhibitors have been reported to enhance AAV production,[32] and the discovery of PLK in AAV production, we focused our further studies on the role of PLKs in AAV manufacturing. We expanded the inhibitor search space to include compounds that target four isoforms of PLK. We found that inhibiting PLK1 and its upstream activator Aurora kinase A/B (AURKA/B)[38–42] enhanced AAV production in adherent HEK293 cells by approximately 2-fold (Figures 2A and 2B).

HMN-214, HMN-176, and rigosertib dose-dependently increased AAV9 capsid titer, vector genome titer, and functional titer in suspension HEK293 cells

We tested how three PLK1 inhibitors affect AAV production in suspension HEK293 cells. These inhibitors included HMN-214,

Figure 1. High-throughput screen identifies compounds that improve AAV9 production

(A) Schematic overview of high-throughput screen to identify compounds that increase AAV9 production. Compounds were added at the time of triple-transfection using pHelper, RepCap9, and an inverted terminal repeat (ITR)-containing reporter vector. (B) A small-molecule screen of bioactive compounds was performed at a 1-μM dose on HEK293F cells. AAV9 capsid titer was measured with ELISA 3 days after triple-transfection and normalized to DMSO. The top-performing compounds (3σ above the DMSO mean) that increased the AAV9 capsid titer can be clustered into five pathways or target classes: cell cycle modulators, G protein-coupled receptor (GPCR), histone deacetylase (HDAC), Janus kinase (JAK) inhibitors, and metabolic targets. (C) Heatmap of the top-performing AAV9 small molecules from the primary screen were examined in a confirmation study in which HEK293F cells were treated with four doses of each small-molecule. Adding HMN-214 (PLK1 inhibitor) and four microtubule inhibitors (vindesine sulfate, combretastatin A4, monomethyl auristatin E [MMAE], and ansamitocin p-3) at the time of triple-transfection enhanced AAV9 production. (D) Relative AAV9 functional titer was measured using a cell-based assay, and data were plotted against the capsid titer. The top-performing compounds that improved both capsid titer and functional titer were HMN-214 and combretastatin A4.

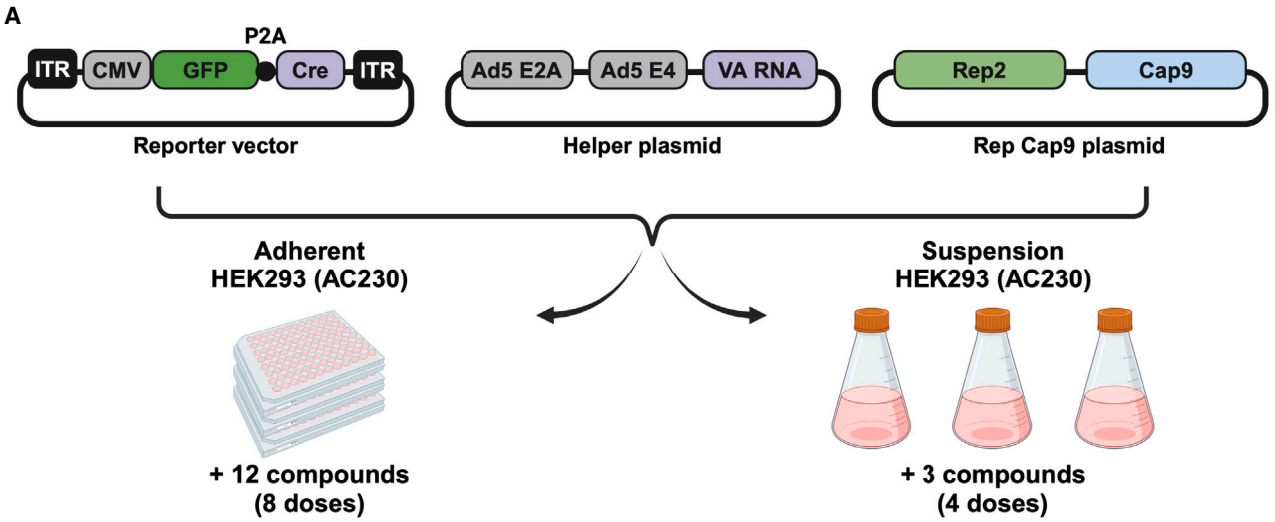

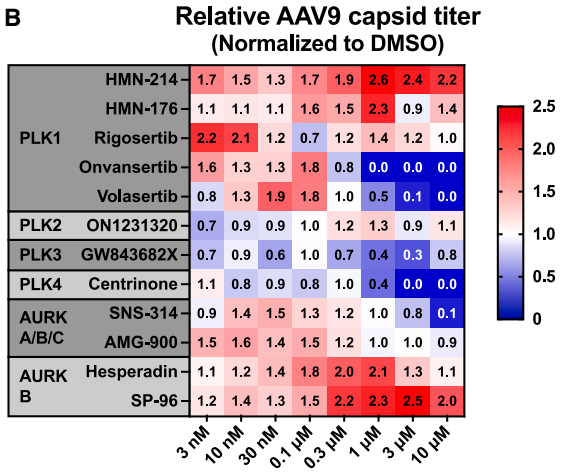

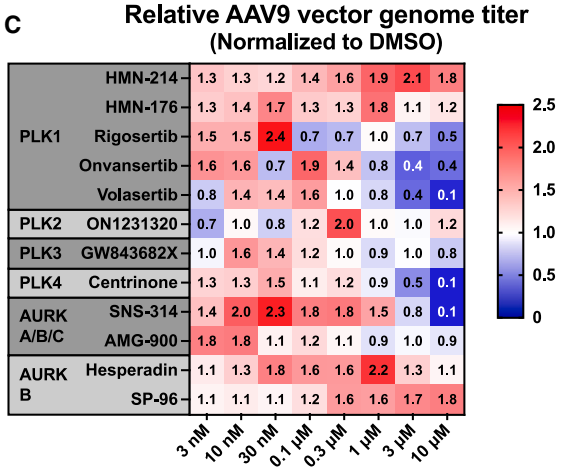

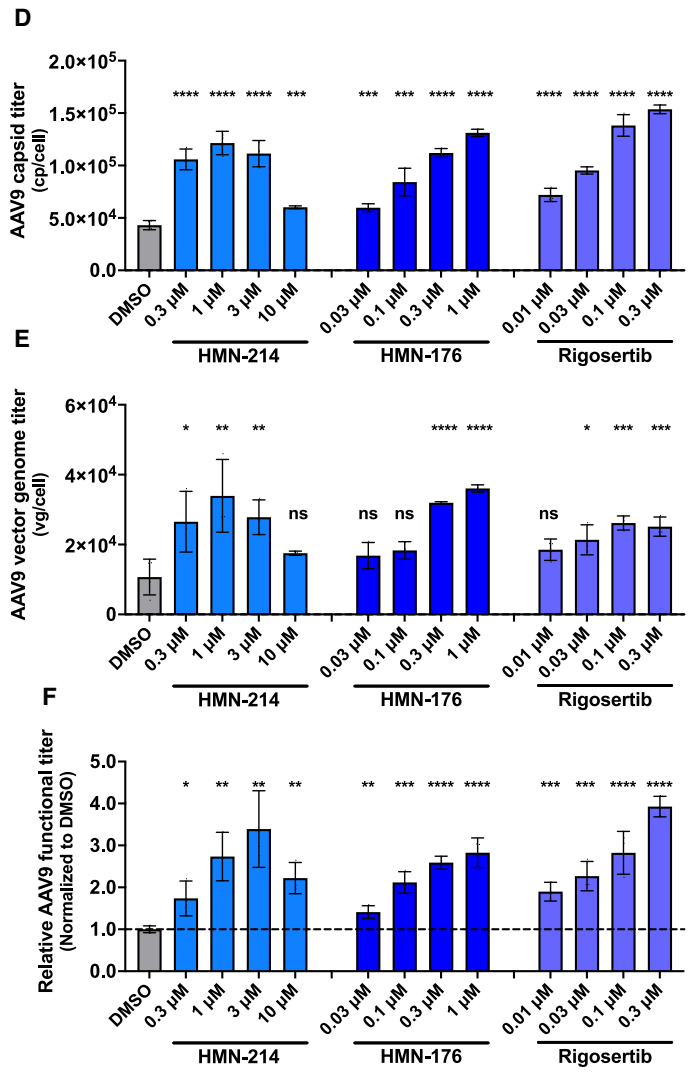

(legend on next page)

HMN-176 (an active metabolite of HMN-214),[43] and rigosertib (a structurally different PLK1 inhibitor).[44] We added these PLK1 inhibitors at the time of triple-transfection in suspension HEK293 cells. Inhibiting PLK1 using these compounds resulted in a dose-dependent increase in AAV9 production measured by capsid titer, vector genome titer, and functional titer (Figures 2D–2F). Because the performance did not significantly differ among these PLK1 inhibitors, and HMN-214 was first identified in the primary screen, we focused our further studies on HMN-214 as a tool compound. Notably, treatment with HMN-214 resulted in an increase in AAV9 capsid titer, both within cells and in AAV secreted into the cell culture media (Figure S2C).

To confirm that greater AAV titers were not due to higher transfection efficiency, we measured the transfection signal in HEK293 cells with and without HMN-214 using two-plasmid reporter transfections (mCherry and GFP) (Figure S2D). We found that HMN-214 did not significantly alter plasmid transfection efficiency (Figures S2E and S2F), which suggests that enhancement in AAV9 production is not due to an increase in transfection efficiency.

HMN-214 increases AAV9 titer using a split two-plasmid system in the Ambr15 microbioreactor

To ensure translatability of our findings to a bioreactor system, we tested different doses and timings of HMN-214 treatment using an Ambr15 microbioreactor. For these studies, we used an AAV9 split two-plasmid system described previously.[45] In this split two-plasmid system, one plasmid carries the ITR-containing reporter with Cap9 and the other plasmid carries the Helper elements and Rep2 (Figure 3A). We transfected the split two-plasmids into suspension HEK293 cells in the Ambr15 microbioreactor. To determine the optimal timing for HMN-214 addition, cells with HMN-214 at various time points (0 h; 4 h; and 0, 24, and 48 h) during AAV9 production (Figure 3A). When we tested the doses of HMN-214 (range, 0.3–10 μM), we noticed a dose-dependent increase in AAV9 vector genome titer at doses up to 3 μM, with maximal efficacy at 1 μM. However, these titers dropped at higher doses of HMN-214 (6 and 10 μM), possibly due to reduced cell viability at these concentrations (Figures 3B and 3C). Host cell DNA, Cap, and kanamycin resistance gene (Kan^R) DNA impurities dose-dependently increased with higher doses of HMN-214 (Figures S3B–S3D).

Our initial Ambr15 study suggested the optimal timing for inhibiting PLK1 to increase AA9 yields is at the point of transfection. We subsequently validated these findings in follow-up studies using the split two-plasmid transfection system, applying the optimal dose and timing of HMN-214 (1 μM at 0 h). In all these studies, the capsid titer was an average of 2.8-fold higher, and the vector genome titer was an average of 2.9-fold higher in cells treated with HMN-214 vs. DMSO control (Figures 3E and 3F). However, the Vg:Cap ratio did not differ between groups (Figure 3G).

HMN-214 increases AAV9 production in multiple HEK293 cell lines

To confirm that our findings with HMN-214 were not limited to one specific HEK293 cell line, we tested its effects on AAV9 production across HEK293 cells from four different sources (materials and methods and Table S2). We developed clonal cell lines using the Solentim VIPS PRO Single Cell Seeder,[46] and included a number of clones for this study. We then treated the HEK293 cell lines with the most efficacious dose of HMN-214 from our previous studies (1 μM) in both shake flasks and Ambr15 bioreactors. We found that HMN-214 treatment increased AAV9 production in several polyclonal and clonal cells lines (Figures 4A, 4B, S4A, and S4B), supporting that HMN-214 enhances AAV9 production in HEK293 cells from different sources.

HMN-214 increases AAV9 production using vectors expressing therapeutic transgenes

We tested the effects of HMN-214 on three additional vectors containing therapeutically relevant transgenes with approved gene therapy products (F9, SMN1, RPE65). To minimize the confounding effects of promoter choice and regulatory elements on AAV yields, we used the same vector design for all vectors and only changed the sequence of the transgene of interest. With our triple-transfection method, we found that HMN-214 significantly increased the AAV9 vector genome titer approximately 2-fold when using vectors expressing therapeutic transgenes (Figure 4C).

HMN-214 increases AAV production in multiple serotypes

Next, we measured whether HMN-214 enhances production of other AAV serotypes. We triple-transfected HEK293 cells with multiple AAV serotypes (1–9 and Rh10) and treated these cells with HMN-214 at the time of transfection. HMN-214 significantly increased both the vector genome titer and functional titer across all tested serotypes, except AAV3 (Figures S4C and S4D). For AAV3, HMN-214 significantly increased the vector genome titer (Figure S4C) but not the functional titer (Figure S4D). This difference may be because we optimized the functional titer assay for AAV9, which was the primary focus of our initial screen. As a result, the functional titer assay may have different sensitivities to different AAV serotypes, potentially influencing the observed differences. Nonetheless, our findings

Figure 2. HMN-214, HMN-176, and rigosertib dose-dependently increased AAV9 capsid titer, vector genome titer, and functional titer in suspension HEK293 cells

(A) Schematic overview of study to measure the effects of PLK and Aurora kinase inhibitors on AAV9 production in adherent and suspension cells. (B) AAV9 capsid and (C) vector genome titers are displayed as a heatmap relative to the DMSO control. Inhibition of PLK1 and Aurora kinase enhanced AAV9 production by approximately 2-fold higher than baseline in adherent HEK293 cells. Adding HMN-214, HMN-176, and rigosertib (PLK1 inhibitors) at the time of triple-transfection led to a dose-dependent increase in AAV9 production in suspension HEK293 cells. AAV9 production was measured based on (D) capsid titer, (E) vector genome titer, and (F) relative functional titer. Data are shown as mean ± SD. $^*p < 0.05$, $^{**}p < 0.01$, $^{***}p < 0.001$, and $^{****}p < 0.0001$. DMSO, dimethyl sulfoxide; ns, not significant.

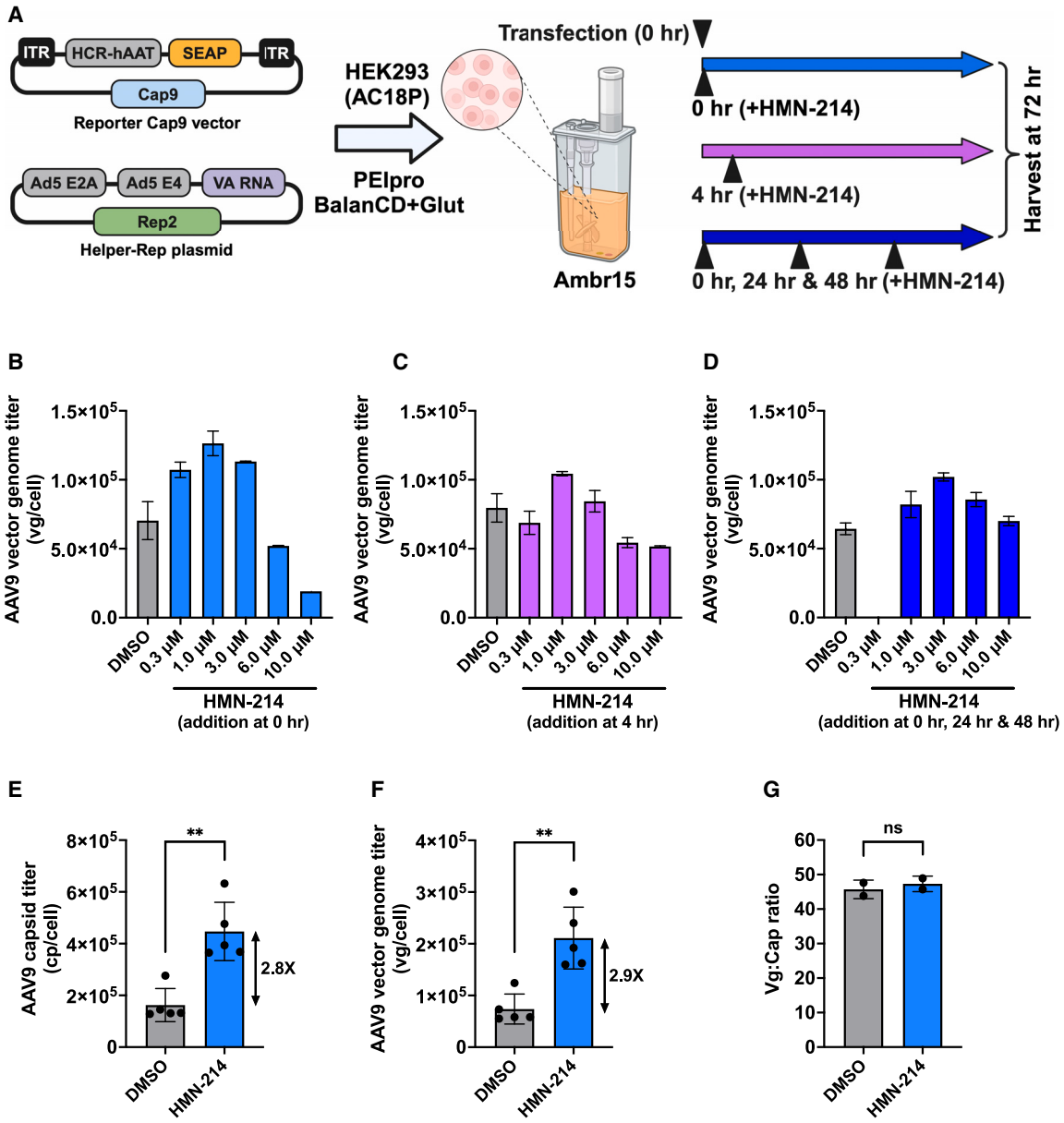

Figure 3. HMN-214 increases AAV9 titer in a split two-plasmid system in the Ambr15 microbioreactor

(A) Schematic overview of confirmatory studies in the Ambr15 microbioreactor using a split two-plasmid system evaluating the effects of HMN-214 on AAV9 production. HMN-214 was added at various times (0 h; 4 h; and 0, 24, and 48 h) during AAV9 production. (B–D) AAV9 vector genome titer increased in a dose-dependent manner up to 1 μM of HMN-214 and declined at higher doses. Data from independent Ambr15 studies show an average of ∼2.8-fold increase in AAV9 (E) capsid titer and (F) vector genome titer using HMN-214 (1 μM, addition at 0 h). (G) The Vg:Cap ratio did not differ with HMN-214 treatment. Data are shown as mean ± SD. Statistical analysis was performed using the Student's t test. *$p < 0.05$, **$p < 0.01$, ***$p < 0.001$, and ****$p < 0.0001$. ITR, inverted terminal repeat; ns, not significant.

suggest that HMN-214 increases AAV production independent of the AAV capsid when using triple-plasmid transfection.

HMN-214 slows growth of HEK293 cells by halting cells in the G2/M phase and blocking exit from the M to G1 phase

Given the role of PLKs in cell cycle progression,[40,47] we explored the mechanism by which PLK inhibitors may lead to higher AAV titers. First, we looked at the growth rate of HEK293 cells after transfection and treatment with different doses of HMN-214. We found that adding HMN-214 slowed the growth of HEK293 cells (Figure 5A) at a rate that anticorrelated with AAV9 capsid titer after transfection (Figure 5B).

To further interrogate the effects of HMN-214 on the cell cycle, we assayed cell proliferation with dual DNA content and EdU flow

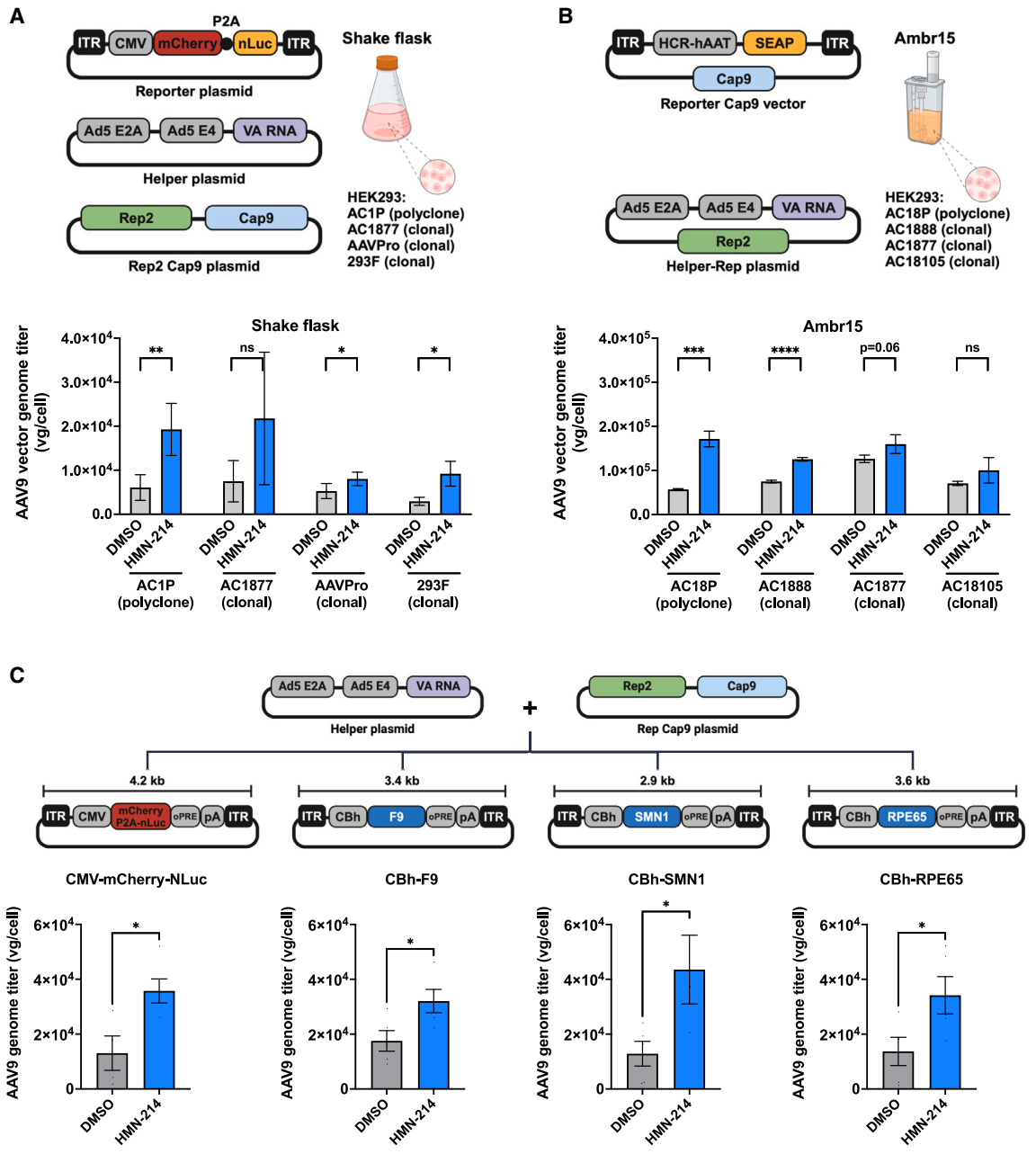

Figure 4. HMN-214 increases AAV9 titer in clonal HEK293 cells and vectors containing therapeutic transgenes

(A) AAV9 production was performed using different HEK293 cells in shake flasks. Cells were transfected with the triple-plasmid system and HMN-214 (1 μM) was added at the time of transfection. HMN-214 increased AAV9 vector genome titer in a polyclonal HEK293 cell line (AC1P) and two clonal lines (AAVPro and 293F). AAV9 titers increased in the third clonal cell line (AC1877); however, the effect size was not statistically significant. (B) AAV9 production was performed using different HEK293 cells in the Ambr15 microbioreactor system. Cells were transfected with the split two-plasmid system and HMN-214 (1 μM) was added at the time of transfection. HMN-214 increased AAV9 vector genome titer in a polyclonal HEK293 cell line (AC18P) and two clonal lines (AC1888 and AC1877). AAV9 titers did not significantly increase in the third clonal cell line (AC18105). (C) AAV9 production was performed in shake flasks using different vectors carrying therapeutic transgenes (F9, SMN1, RPE65) along with mCherry-P2A-NLuc control vector. Cells were triple-transfected, and HMN-214 (1 μM) was added at the time of transfection. HMN-214 significantly increased AAV9 vector genome titers of other vectors containing therapeutic transgenes. Data are shown as mean ± SD. Statistical analysis was performed using the Student's t test. $^{*}p < 0.05$, $^{**}p < 0.01$, $^{***}p < 0.001$, and $^{****}p < 0.0001$. ns, not significant.

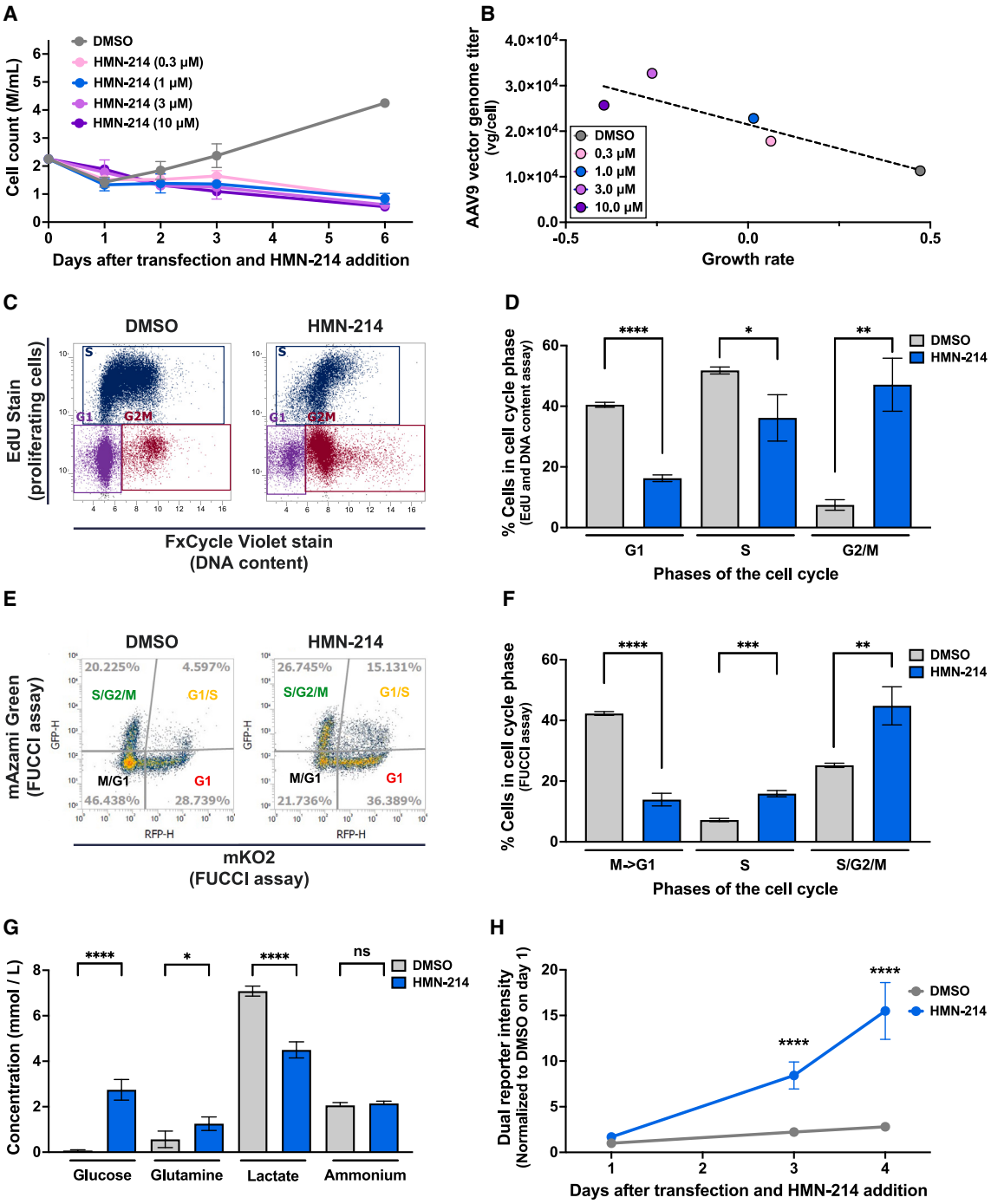

Figure 5. HMN-214 slows the growth rate of HEK293 cells by blocking cell cycle progression from the M to G1 phase

(A) HEK293 cells were triple-transfected with a pHelper, RepCap9, and ITR-containing reporter vector. Samples were treated with either DMSO or HMN-214 at the time of transfection, and the cell count was monitored over time. The DMSO-treated condition shows a slightly lower cell count after transfection, but the cells continued to grow after day 3. HMN-214-treated cells showed a slow decline in cell number over time. (B) AAV9 capsid titer was measured in DMSO-treated or HMN-214-treated samples on day 3 after triple-transfection and plotted against the rate of cell growth. The AAV9 capsid titer was anticorrelated with the cell growth rate. HMN-214 (1 μM) treatment (C) reduced the percentage of proliferating cells (EdU-positive) and (D) increased the fraction of cells in the G2/M phase (EdU-negative, double-DNA content). A fluorescent ubiquitination-based cell cycle indicator (FUCCI) reporter cell line was used to analyze cell proliferation and cell cycle states in various treatment groups. Groups treated with HMN-214

(legend continued on next page)

cytometry. HMN-214 treatment reduced the percentage of proliferating cells (EdU-positive) and increased the fraction of cells in the G2/M phase (EdU-negative, double-DNA content) (Figures 5C and 5D). We also developed a reporter cell line by integrating a fluorescent ubiquitination-based cell cycle indicator (FUCCI) reporter into HEK293 cells (Figures S5A–S5C). Then we used clonal FUCCI HEK293 cells (AC1555) to analyze cell cycle states during treatment with HMN-214. When cells were treated with HMN-214, a lower fraction of FUCCI HEK293 cells were in the M/G1 phase and a higher fraction were in the S/G2/M phase than the DMSO control (Figures 5E, 5F, and S5D–S5G).

Next, we measured the media concentrations of metabolic substrates and metabolites in samples treated with or without HMN-214 during AAV9 production. After 3 days, HMN-214-treated samples had significantly higher concentrations of glucose and glutamine in the media, and significantly lower concentrations of lactate. This suggests that reduction in cell growth rate when using HMN-214 leads to reduced glucose consumption, which in turn results in less lactate accumulation compared with the control condition. However, ammonium concentrations did not differ between groups (Figure 5G).

Because active cell cycle progression leads to plasmid dilution, we hypothesized that slowing cell cycle progression and preventing exit from M to G1 should increase expression from transiently transfected plasmids. To test this hypothesis, we performed dual-plasmid transfection (using GFP and an mCherry reporter) and monitored cells for 4 days after transfection and HMN-214 treatment. In DMSO control and HMN-214-treated cells, the average reporter intensity per cell increased approximately linearly with time. However, reporter intensity increased significantly faster with HMN-214 treatment (Figure 5H).

RNA-sequencing analysis identifies differentially expressed pathways associated with HMN-214 treatment

To further interrogate the effects of PLK1 inhibition, we performed RNA-sequencing (RNA-seq) on suspension HEK293 cells (untreated and triple-transfected) treated with and without HMN-214. For each arm of the study, we used three shake flasks and collected samples for RNA-seq analysis before (0 h) and after (24 and 72 h) treatment (Figure S6A). The bioinformatics workflows and statistics on read counts and genome alignment are outlined in Figures S6B and S6C. Analysis of uniform manifold approximation and projection (UMAP) and RNA expression correlation indicated high reproducibility among replicates. These analyses also suggested that timing and exposure to HMN-214, rather than transfection, are the major drivers of transcriptional changes (Figures 6A and S6D).

Inhibition of PLK1 with HMN-214 leads to differential expression of genes involved in cell cycle progression

To explore the regulatory events after HMN-214 treatment, we identified several significantly upregulated and downregulated cellular processes based on a gene ontology (GO) analysis in non-transfected and triple-transfected samples. The GO categories that were significantly upregulated included establishment of mitotic spindle orientation, negative regulation of the cell cycle in the G2/M phase transition, and chromatin assembly. The GO categories that were significantly downregulated included DNA-dependent DNA replication maintenance and replication fork processing (Figure 6B).

Next, we identified the most differentially expressed genes at 24 and 72 h after HMN-214 treatment. Pathway analysis showed that differentially expressed genes modulated transcription (e.g., *ETV1*, *ETV4*, *ETV5*), the stress response (e.g., *HSPA8*, *HSPB8*), cell growth and differentiation (e.g., *GLIPR1*, *H1-0*, *VGF*), the cytoskeleton/actin-binding (e.g., *DNAH17*, *MYO15B*), signal transduction (e.g., *FLIP1*, *DRD4*), the cell cycle and proliferation (e.g., *RBM5*, *ARTN*, *INHA*, *MAPK15*), and the extracellular matrix and adhesion (e.g., *COL4A3*, *HAS2*) (Figures 6C and S6E).

G2/M phase arrest by HMN-214 is associated with modulation of key cell cycle regulators

We narrowed our analysis of cell cycle genes using the Reactome gene set database.[48] For this analysis, we selected a set of 157 genes most often associated with the cell cycle. Of these genes, 92 were differentially expressed either at 24 or 72 h after HMN-214 treatment [$|\log_2$ (fold change)$| > 0.2$; adjusted p value <0.05; Figure S7]. The most highly upregulated genes [($|\log_2$ (fold change)$| > 0.5$] included clustered histone subunits (e.g., *H2AC6*, *H2BC5*), cyclins (e.g., *CCNA2*, *CCNB1*), cell division cycle (e.g., *CDC20*, *CDC26*), *AURKA*, *PLK1*, *PLK2*, and *TP53*. The most significantly downregulated genes included other cell division cycles (e.g., *CDC45*, *CDC7*), anaphase-promoting complex subunits (e.g., *ANAPC2*, *ANAPC4*), cyclin-dependent kinases (e.g., *CDK1*, *CDK2*), cell cycle kinases (e.g., *ATM*, *CHEK2*, *WEE1*), and tubulin isoforms (e.g., *TUBB*, *TUBB4A*, *TUBB4B*) (Figure 6D).

Finally, we aimed to evaluate the interaction of differentially expressed cell cycle transcripts after HMN-214 treatment. We mapped our RNA-seq dataset to the protein-protein interaction network of our curated list of 157 cell cycle genes using the Search Tool for the Retrieval of Interacting Genes/Proteins (STRING) (Figure S8A). This mapping revealed core nodes and clusters of factors that were significantly modulated throughout the cell cycle regulatory network. We also visualized the network with WikiPathways human cell cycle genes (WP179) and mapped this network with our differential

(1 μM) showed (E) fewer cells in the M to G1 phase and (F) more cells in the S/G2/M phase. (G) Substrate and metabolite concentration after 3 days with or without HMN-214 (1 μM) treatment during AAV9 production. (H) Dual reporter intensity (GFP and mCherry) was measured for 4 days after transfection and HMN-214 (1 μM) treatment. GFP and mCherry reporter expression was significantly higher in cells treated with HMN-214 vs. DMSO. Data are shown as mean ± SD. Statistical analysis was performed using the Student's t test. *$p < 0.05$, **$p < 0.01$, ***$p < 0.001$, and ****$p < 0.0001$. DMSO, dimethyl sulfoxide; ns, not significant.

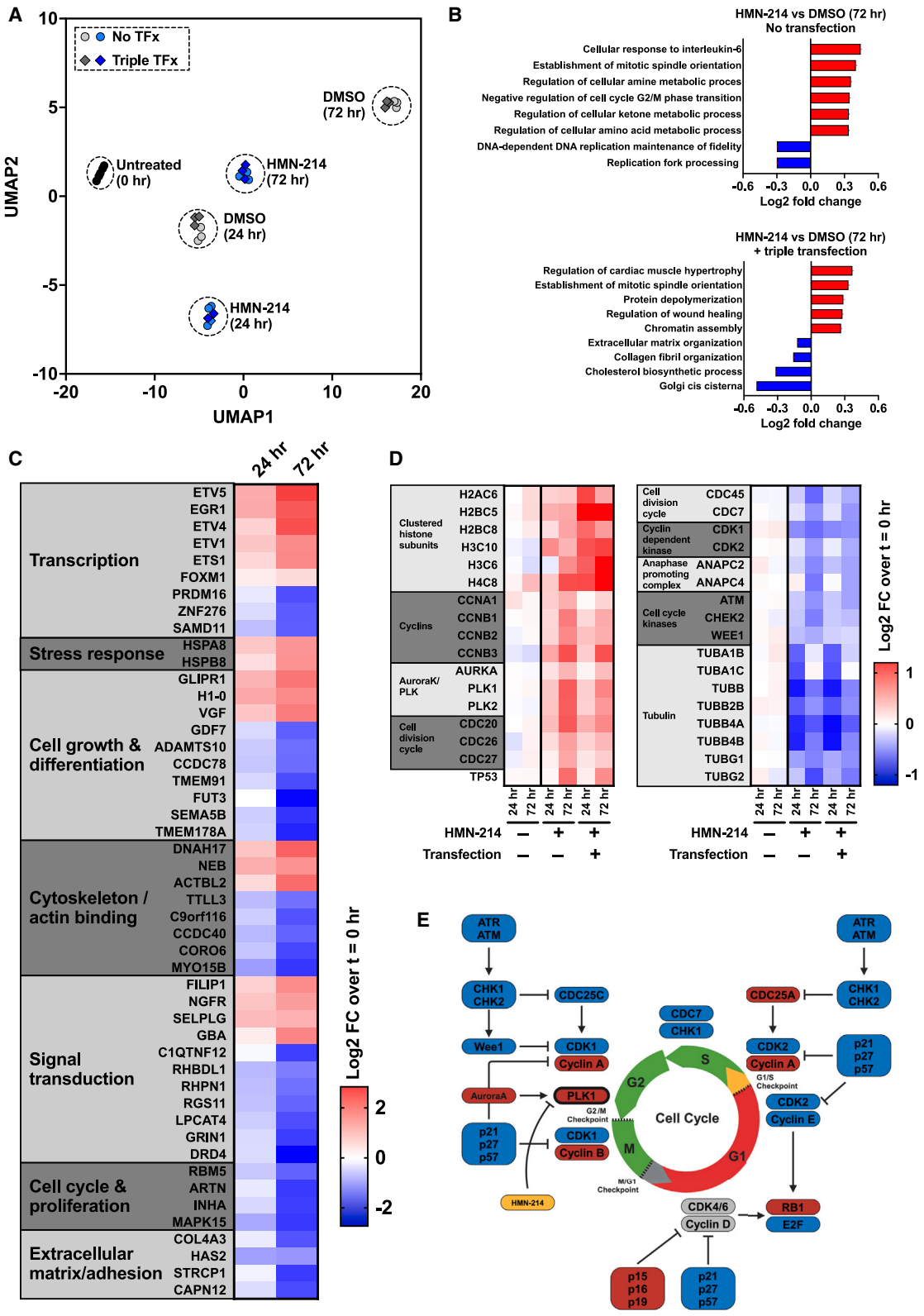

(legend on next page)

expression dataset (Figure S8B). Using these analyses, we developed a simplified model of how inhibiting PLK1 with HMN-214 leads to cell cycle arrest in the G2/M phase and prevents entry to the G1 phase (Figure 6E).

Under normal conditions, PLK1 expression increases during the S phase, and PLK1 phosphorylation of CDC25C and other targets is required for mitotic entry.[49] With HMN-214 treatment, PLK1-dependent phosphorylation is blocked, preventing the G2/M transition. HMN-214 also alters expression of *CDC25C* and several other PLK1 interactors, further contributing to G2/M arrest. Notably, HMN-214 downregulates genes encoding several key subunits of the anaphase-promoting complex (e.g., *ANAPC1/2/4/7*) and upregulates genes encoding cohesin complex subunits (e.g., *SMC1/3*, *STAG1/2*). Also, HMN-214 treatment downregulates genes encoding upstream negative regulators of PLK1 (e.g., *ATM/ATR, CHK1/2*). We also found that HMN-214 upregulates the transcription factor *FOXM1*, and its targets (e.g., *AURKA, CCNB1*), as well as *PLK1* itself (Figures 6C and 6D). These findings collectively suggest a feedback regulatory mechanism that controls *PLK1* expression and function.[50,51]

DISCUSSION

In this study, we build on previous efforts to improve AAV production and use high-throughput small-molecule screening to identify enhancers of rAAV production. Using the ATLAS platform,[36] we identified putative enhancers of AAV production from a library of approximately 3,300 small molecules. Our primary hits clustered into five pathways or target classes: cell cycle modulators, GPCR modulators, HDAC inhibitors, JAK inhibitors, and metabolic modulators. Most prominently, the PLK1 inhibitor HMN-214 increased AAV9 production by arresting cells in the G2/M phase and preventing cell cycle progression from the M to G1 phase. The increase in AAV production was largely consistent across different HEK293 cell lines and clones, vector payloads, and capsid serotypes. These findings support that inhibiting PLK1 may enhance AAV production regardless of cell line, serotype, or vector payload.

PLKs are important regulators of the DNA-damage response, cell cycle progression, spindle formation, and cytokinesis.[42] As a result, several PLK inhibitors are being developed as anti-cancer medicines.[47,52,53] PLKs consist of five paralogues, of which PLK1 is the most studied.[52] PLK1 localizes to centrosomes during G2, then at kinetochores and the spindle pole during metaphase. PLK1 is required for mitotic entry during recovery from G arrest induced by DNA damage.[42,52,54] Also, when PLK1 is inhibited, cells enter mitotic arrest.[55]

We confirmed the effects of HMN-214 on cell cycle arrest in the G2/M phase and in blocking progression from the M to G1 phase. In line with these findings, transcriptional profiling and GO analysis showed that inhibiting PLK1 led to differential expression of genes involved in mitotic spindle orientation, negative regulation of the G2/M phase transition of the cell cycle, and chromatin assembly. In addition, approximately 80% of transcripts involved in cell cycle regulation were differentially expressed after HMN-214 treatment. Of these genes, the most significantly upregulated encode histone subunits, cyclins, cell division cycle genes, *AURKA*, *PLK1*, and *PLK2*. Conversely, the downregulated genes were involved in anaphase promotion, cyclin-dependent kinases, cell cycle kinases, and tubulins. With these findings and further network analysis, we developed a model for how PLK1 inhibition with HMN-214 induces cell cycle arrest in the G2/M phase to prevent progression to G1.

Our small-molecule screen identified other cell cycle modulators (e.g., Wee1, HER2, MEK1 inhibitors), as well as previously reported microtubule and HDAC inhibitors,[32,56] as enhancers of AAV production. Also, several recent RNA-seq studies identified key cellular pathways that may be important for AAV production. These pathways include stress, inflammatory, and immune response (e.g., Toll-like receptor, JAK-STAT, unfolded protein response, heat-shock); metabolic and amino acid transport; nucleosome components; and cell cycle regulators.[57–60] However, RNA-seq alone cannot reveal whether transcriptional changes in these pathways promote or inhibit viral production, or if these changes are a downstream response to upstream regulators altered during AAV production.[57] In the case of cell cycle modulation, our small-molecule screen combined with RNA-seq revealed that arresting cells in G2/M via PLK1 inhibition results in downstream transcriptional changes that further prevent cells from progressing through mitosis. These findings support that cell cycle regulation is essential for enhancing AAV yields using transient transfection. Arresting cells at the G2/M phase after transfection likely frees cellular resources for viral capsid packaging and preventing plasmid dilution through cell division. This aligns with the observed inverse relationship between cell growth and rAAV production, suggesting that as cell division slows, fewer resources are

Figure 6. Inhibition of PLK1 with HMN-214 leads to differential expression of genes involved in cell cycle progression

(A) UMAP analysis indicates high reproducibility among replicates and suggests that exposure to HMN-214, rather than transfection, was the major driver of transcriptional changes. (B) Significantly upregulated gene ontology (GO) terms with HMN-214 treatment included establishment of mitotic spindle orientation, negative regulation of cell cycle G2/M phase transition, and assembly of chromatin. Significantly downregulated GO categories included DNA-dependent DNA replication maintenance and replication fork processing. (C) Pathway analysis of differentially expressed genes at 24 and 72 h after HMN-214 exposure revealed modulation of genes related to transcription, the stress response, cell growth and differentiation, the cytoskeleton/acting-binding, signal transduction, the cell cycle and proliferation, and the extracellular matrix and adhesion. (D) The most highly upregulated cell cycle-associated genes after HMN-214 treatment included clustered histone subunit genes, cyclins, cell division cycle genes, *AURKA*, *PLK1*, *PLK2*, and *TP53*. The most downregulated genes included cell division cycle genes, anaphase-promoting complex subunits, cyclin-dependent kinases, cell cycle kinases, and tubulin isoforms. (E) Simplified model summarizing how Polo-like kinase 1 (PLK1) inhibition with HMN-214 leads to cell cycle arrest in the G2/M phase and prevents entry to the G1 phase. Red, upregulated genes; blue, downregulated genes.

required for biomass maintenance, making more available for processes dedicated to viral vector production. Arresting cell cycle progression may also help maintain the optimal stoichiometric ratio of plasmids, contributing to higher AAV titers.

Our findings are supported by recent transcriptomic and proteomic analyses of PLK1 inhibition.[51,61] Thus, inhibiting PLK1 and PLK1-interacting proteins may have synergistic effects on AAV production. For example, p53 activation can reduce cell sensitivity to PLK1 inhibition,[62] and p53 was strongly upregulated in our HMN-214-treated samples. Also, PLK1 inhibition led to downregulation of CDC7, a downstream effector of PLK1 that is involved in maintaining DNA replication forks.[61] Furthermore, PLK1 inhibition is genetically enhanced by spindle assembly and chromosomal attachment/segregation factors.[63] The dysregulation of these components in our dataset suggests that they could be targeted along with HMN-214 treatment to further enhance AAV output by arresting cells at G2/M.

In our screen, we identified some inhibitor classes (e.g., PLK, Aurora Kinase, and JAK inhibitors) that were previously reported to increase AAV transduction efficiency.[64]

Although we did not evaluate the effect of our lead small-molecule AAV production enhancers on AAV transduction efficiency, these inhibitor classes may share mechanisms for increasing both AAV production and transduction. These possible shared mechanisms warrant further investigation.

Our study has a few limitations. First, the small-molecule library we used for our screen is enriched in anti-cancer compounds that affect the cell cycle. Due to the limited diversity in the chemical space, our screen does not cover all potential pathways and targets that may influence AAV production. Second, our screen was performed at a single dose (1 μM), which constrained our ability to identify small molecules that are efficacious at concentrations higher or lower than the tested dose. Third, we potentially further enhanced AAV yields by incorporating additional compounds identified in our primary and confirmatory studies (e.g., GPCR modulators, JAK, Aurora kinase, microtubule, HDAC inhibitors) alongside PLK1 inhibition. To support this effort, identified targets could be temporarily modulated in producer cell lines using genetic circuits, CRISPR-Cas9-based knockout, or siRNA/shRNA knockdown strategies during AAV production. Fourth, the scalability of our findings needs to be validated in larger-scale production bioreactors. Fifth, the long-term stability and safety of AAV produced with these small-molecule enhancers needs to be assessed. Last, the economic feasibility of integrating these small-molecule enhancers into an existing manufacturing workflow needs further consideration. Addressing these limitations will be crucial for advancing AAV production and making gene therapies more accessible.

In conclusion, our study highlights the power of our high-throughput screening method to identify putative enhancers of AAV production. Through several studies, we validated that chemically inhibiting PLK1 enhanced AAV9 yields with different PLK1 inhibitors, HEK293 cell lines, AAV serotypes, triple and split two-plasmid systems, transgene payloads, and production formats (adherent, suspension shake flask, and Ambr15 micro-bioreactor). Our findings show that inhibiting PLK1 during the biomanufacturing process can significantly increase AAV yields for research, preclinical applications, and potentially good manufacturing practices. As the demand for AAV-based therapies continues to grow, this strategy could enhance AAV production and provide more cost-effective methods for manufacturing AAV for gene therapies.

MATERIALS AND METHODS

Information on cell lines, media, compounds, and kits used in this study are listed in Table S2.

Adherent and suspension adaptation of HEK293 cells

Adherent HEK293 cells were expanded in Dulbecco's Modified Eagle's Medium (DMEM), high glucose, GlutaMAX Supplement, pyruvate (Thermo Fisher Scientific, Waltham, MA) supplemented with 10% fetal bovine serum (Thermo Fisher Scientific, Waltham, MA) in a 37°C, 5% CO_2 incubator. Once cells reached approximately 80% confluence, the media was carefully aspirated and replaced with BalanCD HEK293 media (FUJIFILM Irvine Scientific, Santa Ana, CA). Then the cells were incubated for 48 h in the adherent format at 37°C, 5% CO_2. After 2 days in BalanCD HEK293 media, cells were resuspended in 2 mL fresh media and placed on an orbital shaker (125 rpm, 19-mm orbital throw) in a 37°C, 5% CO_2 incubator. After 2 days in suspension, cell viability and density were measured using a Countess 3 and Trypan Blue (Thermo Fisher Scientific, Waltham, MA), and cells were maintained at 0.5–5 E6/mL. After 9 days in suspension, cells were transferred to 125-mL shake flasks. All cell lines were negative for mycoplasma based on the MycoAlert Mycoplasma Detection Kit (Lonza, Cambridge, MA).

Maintenance of HEK293 cells in suspension before transfection

Suspension HEK cells were maintained in BalanCD HEK293 media on an orbital shaker (125 rpm, 19-mm orbital throw) in a 37°C, 5% CO_2 incubator. Cell growth and viability were monitored for 7–10 days until cells reached a density of 2.5–5E6/mL and >95% viability before transfection. Cells were then centrifuged at 500 × g for 5 min. Spent media was aspirated, and the cell pellet was resuspended in the appropriate volume of BalanCD HEK293 media to achieve a density of 2.5E6/mL in a 125-mL shake flask.

AAV production using triple-transfection

The triple-transfection system used a pHelper and RepCap plasmid (#6234, Takara Bio, Shiga, Japan), and an ITR-containing reporter plasmid. The pHelper plasmid contained Ad5 E4, Ad5 E2A, and Ad5 VA-RNA. The RepCap plasmid expressed AAV2-derived Rep78 and Rep68 under the control of the P5 promoter; and Rep52 and Rep40 under the control of the P19 promoter. Serotype-specific AAV Cap sequence containing VP1, VP2, and VP3 were synthesized (Twist Bioscience) and cloned into the RepCap plasmid (#6234, Takara Bio, Shiga, Japan) under the control of the P40 promoter. The

ITR-containing reporter plasmid expressed mCherry-P2A-NLuc under the control of a CMV promoter. Samples (cells and media) were harvested 72 h after transfection and lysed using AAV-MAX lysis buffer (Thermo Fisher Scientific, Waltham, MA) for AAV titer analysis.

High-throughput compound library screen

pHelper plasmid, RepCap9 plasmid, and the ITR-containing reporter vector were prepared at a 1:1:1 M ratio. The DNA mix was then diluted in phosphate-buffered saline (PBS) to obtain a volume of 10% of the total culture volume and a final concentration of 3.0 μg/mL. Next, room temperature TransIT-VirusGEN (Mirus Bio, Madison, WI) transfection reagent was added to the diluted DNA at two times the volume of the diluted DNA mix (2:1 transfection reagent to total DNA) and incubated for 15 min at room temperature. Then the TransIT-VirusGEN:DNA was added to a shake flask containing HEK293F cells at a density of 2.5E6/mL and incubated for 4 h. Next, transfected cells were diluted 1:5 with BalanCD HEK293 media to obtain a cell density of 0.5E6/mL. Using a multichannel liquid handler, 90 μL of cells were seeded per well of a 96-well plate to obtain a final cell density of 50,000 cells/well. A compound library of bioactive small molecules (Food and Drug Administration-approved and passed phase 1 drug library; Selleckchem, Houston, TX) was diluted to create a working library at a concentration of 10 μM. Using a multichannel liquid handler, 10 μL of the 10 μM working library was added to each well and mixed five times to obtain a final drug concentration of 1 μM per well. Plates were then incubated at 37°C in a 5% CO_2 incubator for 72 h with no media change before harvesting samples. Then, 3 days after transfection and compound addition, samples (cells and media) were harvested and lysed using AAV-MAX lysis buffer (Thermo Fisher Scientific, Waltham, MA). AAV9 capsid titer was determined with ELISA.

Determination of capsid titer from shake flask studies with ELISA

A streptavidin-coated, high-capacity plate (Thermo Fisher Scientific, Waltham, MA) was coated for 1 h at room temperature with the CaptureSelect Biotin anti-AAV9 conjugate (Thermo Fisher Scientific, Waltham, MA) at a dilution of 1:10,000 in PBS +0.1% Tween 20 (PBST). After incubation, the capture antibody solution was aspirated from each well of the plate, and each well was washed three times with 150 μL PBST. Then 100 μL of either standard or sample was added to the plate. A 5- to 7-point standard was used in all studies with the AAV9 empty capsid standard (Progen, Heidelberg, Germany). The plate was covered with foil-sealing film and incubated on a shaker for 1 h at room temperature. After incubation, the entire sample was aspirated, and the plate was washed three times with 150 μL PBST. CaptureSelect horseradish peroxidase anti-AAV9 conjugate (Thermo Fisher Scientific, Waltham, MA) was diluted 1:50,000 in PBST, and 100 μL of the diluted detection antibody was added to each well. The plate was covered with foil-sealing film and incubated on a shaker for 1 h at room temperature. After incubation, the horseradish peroxidase anti-AAV9 conjugate solution was aspirated and washed three times with 150 μL PBST. Then 100 μL TMB ELISA substrate (highest sensitivity; Abcam, Waltham, MA) was added per well and incubated for 2–5 min before adding 100 μL of ELISA Stop Solution (Thermo Fisher Scientific, Waltham, MA). Absorbance was measured on the Varioskan microplate reader at 450 nm (Thermo Fisher Scientific, Waltham, MA).

Determination of vector genome titer from small-scale studies with quantitative PCR

Purified or crude viral supernatant was treated with DNase I for 90 min at 37°C according to manufacturer's instructions (New England BioLabs, Ipswich, MA). Quantitative PCR was performed using a custom fluorescein amidites probe against Nano Luciferase (Thermo Fisher Scientific, Waltham, MA) and TaqMan Fast Advanced Master Mix (Thermo Fisher Scientific, Waltham, MA) on a QuantStudio 6 Flex Real-Time PCR System (Thermo Fisher Scientific, Waltham, MA). Plasmid DNA was used at concentrations from 0.0001 to 1 ng/μL to generate a standard curve.

AAV harvest and purification from small-scale studies

Cells were lysed via three rounds of freezing on dry ice followed by thawing at 37°C. After mixing lysed samples, cell debris was removed by centrifuging at 1000 × *g* for 10 min, and AAV-containing supernatant was saved for processing and stored at −80°C.

Confirmation studies in suspension HEK293 cells

Confirmation studies were performed in suspension using four lines of HEK293 cells from different sources: Expi293F (Thermo Fisher Scientific, Waltham, MA), AAVpro 293T (Takara Bio, San Jose, CA), HEK293/"AC18P" (DSMZ, Braunschweig, Germany), and HEK293/"AC1P" (Cytion, Eppelheim, Germany). Additional details about these cell lines are outlined in Table S2. Cells were maintained in suspension in BalanCD HEK293 media (FUJIFILM Irvine Scientific, Santa Ana, CA) supplemented with 4 mM L-glutamine (Thermo Fisher Scientific, Waltham, MA) on an orbital shaker (125 rpm, 19-mm orbital throw) at 37°C in a 5% CO_2 incubator. Cell growth and viability were monitored for 7–10 days until cells reached a density of 2.5–5E6/mL and >95% viability before transfection. Then cells were centrifuged at 500 × *g* for 5 min. Spent media was aspirated, and the cell pellet was resuspended in the appropriate volume of BalanCD HEK293 media to achieve a density of 2.5E6/mL in a 125-mL shake flask.

Transfection mix was prepared as described above, TransIT-VirusGEN:DNA was added to the shake flask with cells at a density of 2.5E6/mL. Compounds were solubilized at a 1000× concentration in DMSO and added to the shake flask at the time of transfection (final concentration of 0.1% DMSO). Shake flasks were then incubated at 37°C in a 5% CO_2 incubator for 72 h with no media change before sample harvest.

rAAV production in Ambr15

rAAV was produced in an Ambr 15 Generation 2 Cell Culture 24 Bioreactor System (Sartorius, Göttingen, Germany). Ambr 15cc bioreactors with sparge were equilibrated with 12 mL of BalanCD

HEK293 media (FUJIFILM Irvine Scientific, Santa Ana, CA) supplemented with 4 mM L-glutamine (Thermo Fisher Scientific, Waltham, MA) at 37°C, 40% dissolved oxygen, and pH set point 7.4. Then 20 μL EX-CELL antifoam (Millipore Sigma, Burlington, MA) was added to each bioreactor every 12 h starting immediately after media fill. To adjust pH levels, 1 M sodium bicarbonate solution was used. HEK293 suspension cells were seeded into Ambr 15cc bioreactors at a final concentration of 2.5 M/mL. Cells were transfected with the split two-plasmid system[45] (4:3 M mixture of Helper and vector plasmid) using the linear polyethylenimine transfection reagent PEIpro (Polyplus, Illkirch, France) according to the manufacturer's instructions. Per viable cell, a total plasmid DNA amount of 0.52 pg was applied. The PEIpro-DNA complexes were prepared in BalanCD HEK293 media supplemented with 4 mM L-glutamine. HMN-214 was added to respective bioreactors in BalanCD HEK293 media at a final concentration of 0.1% DMSO. Cells were cultured for 3 days after transfection, followed by harvest and lysis with three freeze-thaw cycles (−80°C and 37°C). Cell debris was removed by centrifuging at 3,700 × *g* for 30 min at 4°C. Cell lysates underwent a nuclease treatment procedure to remove extra-particulate DNA. For this procedure, the samples were treated by adding Denarase endonuclease (c-LEcta, Leipzig, Germany) at a final activity of 0.02 U/μL and incubating at room temperature for at least 12 h. Then, samples were centrifuged at 1000 × *g* for 10 min to remove any precipitate arising from the treatment and supernatant was retained.

rAAV purification from Ambr15

rAAV particles were purified from the Denarase-treated cell lysates using affinity chromatography based on a spin column and applying POROS CaptureSelect AAVX Affinity Resin (Thermo Fisher Scientific, Waltham, MA). We used 150 μL of resuspended affinity resin per cell lysate. Before use, the affinity resin was washed three times with 300 μL of equilibration/wash buffer (20 mM Tris, 100 mM NaCl, pH 7.5). Between wash steps, the affinity resin suspension was centrifuged at 1000 × *g* for 1 min, and supernatants were discarded. After the final centrifugation step, the affinity resin was resuspended in 300 μL of equilibration/wash buffer and transferred to the cell lysate. The mixture was incubated at room temperature for 90 min in an overhead shaker. After incubation, the affinity resin containing captured rAAV was recovered by centrifuging at 1000 × *g* for 1 min and discarding the supernatant. The affinity resin containing captured rAAV particles was transferred to Pierce Cellulose Acetate Filter Spin Cups (Thermo Fisher Scientific, Waltham, MA). The resin was then washed five times with equilibration/wash buffer, with intermittent centrifugation at 1000 × *g*. Finally, the bound rAAV particles were eluted in three rounds, each consisting of adding 100 μL elution buffer (20 mM sodium citrate, 98 mM NaCl, pH 2.5) and then neutralizing the eluate with neutralization buffer (2 M Tris).

Quantification of plasmid-derived impurities from Ambr15

Plasmid-derived impurities were quantified with qPCR for defined sequences of the kanamycin resistance gene (kan^R, on both Helper and vector plasmids) and the AAV Cap gene (on the vector plasmid). These qPCR techniques were performed on the purified material, with modifications to the impurity specific primer pairs, linearized plasmid standards, trending controls, and annealing temperatures in the qPCR setup.

Quantification of host cell-derived impurities from Ambr15

DNA sequences, such as nucleic acid material from the genome of host cells in which AAVs are produced, can be packaged into rAAV particles, which constitutes product-related impurities. Host cell-derived impurities in purified material were quantified with droplet digital polymerase chain reaction (ddPCR) specific for defined sequences of the 18S rRNA gene locus of the 45S ORF present in HEK293 cells.

Substrate and metabolite analysis

Substrate and metabolites were analyzed using the FLEX2 analyzer according to the manufacturer's instructions (Nova biomedical, Waltham, MA).

Click-iT EdU and FxCycle violet for the flow cytometry stain assay

DNA replication in proliferating cells was analyzed with the Click-iT EdU Alexa Fluor 647 Flow Cytometry Assay Kit according to manufacturer's instructions (Thermo Fisher Scientific, Waltham, MA). Briefly, cells were incubated with 50 μM EdU for 1 h, washed once with 1% bovine serum albumin in PBS, fixed with Click-iT fixative for 15 min, washed once with 1% bovine serum albumin in PBS, and permeabilized by resuspending in 1× Click-iT saponin-based permeabilization and wash reagent. Then, cells were incubated in Click-iT detection cocktail for 30 min and washed once with 1× Click-iT saponin-based permeabilization and wash reagent. Next, DNA content in fixed cells was measured using FxCycle Violet stain according to manufacturer's instructions (Thermo Fisher Scientific, Waltham, MA). Two drops of FxCycle Violet Ready Flow Reagent were added to EdU-stained and fixed cells, incubated for 30 min, and protected from light using aluminum foil. Samples were analyzed on the Attune flow cytometer (Thermo Fisher Scientific, Waltham, MA) using the VL1 and RL1 channels.

Generation of a FUCCI cell cycle reporter (AC1555)

A plasmid containing the FUCCI-reporter cassette and a CMV-driven puromycin-selectable marker was synthesized.[65] In this cassette, a CBh promoter drives expression of an mKO2 florescent reporter fused to Cdt1, followed by T2A and mAzami-Green florescent reporter fused to Gem1. Then 1 μg of the FUCCI plasmid was nucleofected into 1E6 HEK293 cells with the 4D-nucleofector transfection system and the SF Cell Line 4D-Nucleofector X Kit S (Lonza, Walkersville, MD). Five days after nucleofection, cells were treated with 5 μM puromycin (Thermo Fisher Scientific, Waltham MA). After 10 days of puromycin selection, the polyclonal population was seeded as single cells using the Solentim VIPS PRO Single Cell Seeder (Advanced Instruments, Norwood, MA). Clones were isolated and verified using microscopy and flow cytometry. A single HEK293 clone (AC1555) was selected based on the amount of reporter

expression and the growth rate for further studies to analyze cell proliferation and cell cycle states in various treatment groups.

Flow cytometry

Suspension HEK293 cells were collected and pelleted at 500 × *g* for 5 min. For each sample, 10,000 live events were captured on the Attune flow cytometer (Thermo Fisher Scientific, Waltham, MA) and analyzed using Attune software.

RNA preparation and sequencing

To characterize RNA expression profiles, suspension AC230 cells were seeded onto six-well plates at a density of 2.5E6 cells/mL in 3 mL of BalanCD HEK293 media with 4 mM L-glutamine. Cells were treated with HMN-214 (1 μM) or 0.1% DMSO control. For each condition, three replicates were triple-transfected for AAV production as described in the "AAV production using triple-transfection" section. For each replicate, 750 μL of cells were removed before transfection and HMN-214 treatment (0 h), as well as 24 and 72 h after treatment. Cells were pelleted, flash frozen, and stored at −80°C. Total RNA was extracted using the Direct-zol-96 RNA Kit (Zymo Research, Irvine, CA) according to the manufacturer's instructions. The RNA concentration was quantified using a NanoDrop spectrophotometer (Thermo Fisher Scientific, Waltham, MA), and RNA quality was assessed via High Sensitivity RNA Screen Tape Analysis (Agilent [Santa Clara, CA]; performed via SeqMatic [Fremont, CA]). Illumina stranded polyA mRNA library preparation and sequencing (NovaSeq X) were performed by SeqMatic (Fremont, CA). On average, 35,425,777.5 ± 2,631,821.5 reads (150-base pair, paired-end) were generated per sample. We deposited our RNA-seq data on the Gene Expression Omnibus (GEO) database: GEO Submission (GSE273692).

Differential expression analysis

We assessed sequence quality using FastQC[66] and trimmed adapter sequences, and low-quality reads using Trimmomatic.[67] Trimmed reads were aligned to the human genome (GRCh38.84) using Hisat2.[68] We then generated gene-level counts of aligned reads using Subread's featureCounts function.[69] On average, Hisat2 aligned 95.9% ± 1.6% of reads to the genome one or more times. Of these reads, 82.3% ± 2.0% were successfully assigned to genomic features.

After obtaining high-quality sequence alignments and counts, we generated an expression matrix and analyzed differential expression with the BigOmics platform.[70] Raw counts were converted into counts per million (CPM) and $\log_2$ normalized for downstream analysis. Genes with at least 1 CPM across two or more samples were included in the analysis. By default, the BigOmics platform uses a combination of statistical tests for differential expression via DESeq2 (Wald), edgeR (QLF), and limma (trend).

Initial UMAP clustering and differential expression tests were performed within the BigOmics web environment, and results were exported for visualization. Correlations between pairwise gene expression of samples were calculated in R using the Pearson method. Multiple contrasts were generated in the BigOmics environment to compare expression profiles between (1) HMN-214 vs. DMSO, (2) triple-transfection vs. no transfection, and (3) 24 vs. 0 h and 72 vs. 0 h timepoints. Unless otherwise noted, we applied a false-discovery rate threshold of 0.01 and a $\log_2$ (fold change) threshold of 0.5 to identify top differentially expressed genes across analyses.

Gene set analysis

To characterize the effects of HMN-214 treatment on gene expression, we performed Reactome pathway analysis[48] using the top differentially expressed genes between samples treated with HMN-214 and DMSO. We identified overrepresented pathways based on a *p* value threshold of 0.05. We then manually curated the results for heatmap visualization by combining overlapping pathways and removing duplicate genes across functional categories. We used a similar approach to classify differentially modulated genes after triple-transfection and AAV production. Also, to identify significantly enriched cellular components and molecular functions after HMN-214 treatment, we performed GO analysis using the BigOmics platform.

Network visualization of cell cycle genes

To visualize how HMN-214 alters expression of cell cycle control genes, we curated a list of 157 human genes identified from Reactome[48] and WikiPathways[71] gene sets related to the cell cycle. We queried this list using the Search Tool for the Retrieval of Interacting Genes/Proteins (STRING)[72] to build an interaction network, with a confidence cutoff of 0.9 and edge thickness corresponding to the combined STRING interaction score. We then merged the node table with our differential expression results (HMN-214 vs. DMSO, 72 h) within the Cytoscape application, mapping node color to the $\log_2$FC and node shape to the adjusted *p* value. To visualize gene modules, we applied the Markov Cluster Algorithm with an inflation value of 2, and we removed clusters with two or fewer genes for visualization. To visualize how our dataset maps onto the canonical cell cycle pathway, we merged the human cell cycle pathway from WikiPathways (WP179) with our full differential expression dataset (HMN-214 vs. DMSO, 72 h), again mapping the node color to $\log_2$FC and the shape to the *p* value.

Statistical analysis

The number of replicates is indicated in the figure legends. Unless otherwise specified, the Student's t test was used for statistical analysis, with significant differences defined as $^{*}p < 0.05$, $^{**}p < 0.01$, $^{***}p < 0.001$, and $^{****}p < 0.0001$. Error bars indicate standard deviation (SD).

DATA AND CODE AVAILABILITY

Our RNA-seq data has been deposited on the GEO database: GEO Submission (GSE273692).

ACKNOWLEDGMENTS

This project was supported by Ascend Advanced Therapies. We thank Crystal Herron of Redwood Ink, LLC for editing the manuscript. We thank H. Griffiths, R. Feitzinger, L. Leveque-Eichhorn, and I. Ukani for assay optimization and plasmid cloning. We thank

Martina Ohme and Elisabeth Schweigert for their technical assistance with analytics and operational support for the Ambr15 runs. Illustrations were created with BioRender.com.

AUTHOR CONTRIBUTIONS

F.G. and M.A.M. were responsible for the conception and design of the experiments. K.F., F.G., F.I., J.T., R.D., and A.S. conducted the experiments. J.T. and M.A.M. performed the RNA-seq analysis and interpreted the results. C.A.R., F.S., M.H., A.S., and M.A.M. supervised the studies. M.A.M. wrote the manuscript with support from all authors.

DECLARATION OF INTERESTS

K.F., F.G., F.I., J.T., R.D., F.S., M.H., A.S., C.A.R., and M.A.M. are employees of Ascend Advanced and have stock holdings in the company. F.G., C.A.R., and M.A.M. are inventors on a patent for methods to enhance AAV production.

SUPPLEMENTAL INFORMATION

Supplemental information can be found online at https://doi.org/10.1016/j.omtm.2025.101412.

REFERENCES

1. Samulski, R.J., and Muzyczka, N. (2014). AAV-Mediated Gene Therapy for Research and Therapeutic Purposes. Annu. Rev. Virol. *1*, 427–451. https://doi.org/10.1146/annurev-virology-031413-085355.
2. Srivastava, A., Lusby, E.W., and Berns, K.I. (1983). Nucleotide sequence and organization of the adeno-associated virus 2 genome. J. Virol. *45*, 555–564. https://doi.org/10.1128/JVI.45.2.555-564.1983.
3. Li, C., and Samulski, R.J. (2020). Engineering adeno-associated virus vectors for gene therapy. Nat. Rev. Genet. *21*, 255–272. https://doi.org/10.1038/s41576-019-0205-4.
4. Kuzmin, D.A., Shutova, M.V., Johnston, N.R., Smith, O.P., Fedorin, V.V., Kukushkin, Y.S., van der Loo, J.C.M., and Johnstone, E.C. (2021). The clinical landscape for AAV gene therapies. Nat. Rev. Drug Discov. *20*, 173–174. https://doi.org/10.1038/d41573-021-00017-7.
5. Senior, M. (2017). After Glybera's withdrawal, what's next for gene therapy? Nat. Biotechnol. *35*, 491–492. https://doi.org/10.1038/nbt0617-491.
6. Reid, C.A., Hörer, M., and Mandegar, M.A. (2024). Advancing AAV production with high-throughput screening and transcriptomics. Cell Gene Therapy Insights *10*, 821–840. https://doi.org/10.18609/CGTI.2024.095.
7. Prasad, R., Lugo, T., Corwin, S., Hanbury-Brown, L., and Boyle, J. (2021). Under the Microscope State of the AAV Gene Therapy Landscape after Recent FDA AdCom on Safety (William Blair Equity Research).
8. Bulcha, J.T., Wang, Y., Ma, H., Tai, P.W.L., and Gao, G. (2021). Viral vector platforms within the gene therapy landscape. Signal Transduct. Targeted Ther. *6*, 53. https://doi.org/10.1038/s41392-021-00487-6.
9. Au, H.K.E., Isalan, M., and Mielcarek, M. (2021). Gene Therapy Advances: A Meta-Analysis of AAV Usage in Clinical Settings. Front. Med. *8*, 809118. https://doi.org/10.3389/fmed.2021.809118.
10. Wang, D., Tai, P.W.L., and Gao, G. (2019). Adeno-associated virus vector as a platform for gene therapy delivery. Nat. Rev. Drug Discov. *18*, 358–378. https://doi.org/10.1038/s41573-019-0012-9.
11. Marks, P., and Witten, C. (2021). Toward a new framework for the development of individualized therapies. Gene Ther. *28*, 615–617. https://doi.org/10.1038/s41434-020-0143-y.
12. Jackson, C.B., Richard, A.S., Ojha, A., Conkright, K.A., Trimarchi, J.M., Bailey, C.C., Alpert, M.D., Kay, M.A., Farzan, M., and Choe, H. (2020). AAV vectors engineered to target insulin receptor greatly enhance intramuscular gene delivery. Mol. Ther. Methods Clin. Dev. *19*, 496–506. https://doi.org/10.1016/j.omtm.2020.11.004.
13. Phillips, M.I., Mohuczy-Dominiak, D., Coffey, M., Galli, S.M., Kimura, B., Wu, P., and Zelles, T. (1997). Prolonged Reduction of High Blood Pressure With an In Vivo, Nonpathogenic, Adeno-Associated Viral Vector Delivery of AT1-R mRNA Antisense. Hypertension *29*, 374–380. https://doi.org/10.1161/01.HYP.29.1.374.
14. Rosenberg, J.B., Kaplitt, M.G., De, B.P., Chen, A., Flagiello, T., Salami, C., Pey, E., Zhao, L., Ricart Arbona, R.J., Monette, S., et al. (2018). AAVrh.10-Mediated APOE2 Central Nervous System Gene Therapy for APOE4-Associated Alzheimer's Disease. Hum. Gene Ther. Clin. Dev. *29*, 24–47. https://doi.org/10.1089/humc.2017.231.
15. Yang, Y., Seok, M.-J., Kim, Y.E., Choi, Y., Song, J.-J., Sulistio, Y.A., Kim, S.H., Chang, M.-Y., Oh, S.-J., Nam, M.-H., et al. (2023). Adeno-associated virus (AAV) 9-mediated gene delivery of Nurr1 and Foxa2 ameliorates symptoms and pathologies of Alzheimer disease model mice by suppressing neuro-inflammation and glial pathology. Mol. Psychiatr. *28*, 5359–5374. https://doi.org/10.1038/s41380-022-01693-6.
16. Greer-Short, A., Greenwood, A., Leon, E.C., Qureshi, T.N., von Kraut, K., Wong, J., Reid, C.A., Cheng, Z., Easter, E., Yang, J., et al. (2024). Gene Therapy Mediates Therapeutic Improvement in Cardiac Hypertrophy and Survival in a Murine Model of MYBPC3-Associated Cardiomyopathy. Preprint at bioRxiv. https://doi.org/10.1101/2024.02.19.581102.
17. Wu, I., Zeng, A., Greer-Short, A., Aycinena, J.A., Tefera, A.E., Shenwai, R., Farshidfar, F., Van Pell, M., Xu, E., Reid, C., et al. (2024). AAV9:PKP2 improves heart function and survival in a Pkp2-deficient mouse model of arrhythmogenic right ventricular cardiomyopathy. Commun. Med. *4*, 38. https://doi.org/10.1038/s43856-024-00450-w.
18. Manso, A.M., Hashem, S.I., Nelson, B.C., Gault, E., Soto-Hermida, A., Villarruel, E., Brambatti, M., Bogomolovas, J., Bushway, P.J., Chen, C., et al. (2020). Systemic AAV9.LAMP2B injection reverses metabolic and physiologic multiorgan dysfunction in a murine model of Danon disease. Sci. Transl. Med. *12*, eaax1744. https://doi.org/10.1126/scitranslmed.aax1744.
19. Tilemann, L., Ishikawa, K., Weber, T., and Hajjar, R.J. (2012). Gene Therapy for Heart Failure. Circ. Res. *110*, 777–793. https://doi.org/10.1161/CIRCRESAHA.111.252981.
20. Smith, J., Grieger, J., and Samulski, R.J. (2018). Overcoming Bottlenecks in AAV Manufacturing for Gene Therapy. Cell Gene Ther. Insights *4*, 815–825. https://doi.org/10.18609/cgti.2018.083.
21. Wright, J.F. (2023). AAV vector production: Troublesome host innate responses in another setting. Mol. Ther. Methods Clin. Dev. *28*, 412–413. https://doi.org/10.1016/j.omtm.2023.02.008.
22. Wang, J.-H., Gessler, D.J., Zhan, W., Gallagher, T.L., and Gao, G. (2024). Adeno-associated virus as a delivery vector for gene therapy of human diseases. Signal Transduct. Targeted Ther. *9*, 78. https://doi.org/10.1038/s41392-024-01780-w.
23. Bennett, A., Mietzsch, M., and Agbandje-McKenna, M. (2017). Understanding capsid assembly and genome packaging for adeno-associated viruses. Future Virol. *12*, 283–297. https://doi.org/10.2217/fvl-2017-0011.
24. Srivastava, A., Mallela, K.M.G., Deorkar, N., and Brophy, G. (2021). Manufacturing Challenges and Rational Formulation Development for AAV Viral Vectors. J. Pharmacol. Sci. (Tokyo, Jpn.) *110*, 2609–2624. https://doi.org/10.1016/j.xphs.2021.03.024.
25. Guan, J.-S., Chen, K., Si, Y., Kim, T., Zhou, Z., Kim, S., Zhou, L., and Liu, X.M. (2022). Process Improvement of Adeno-Associated Virus Production. Front. Chem. Eng. *4*, 830421. https://doi.org/10.3389/fceng.2022.830421.
26. Kimura, T., Ferran, B., Tsukahara, Y., Shang, Q., Desai, S., Fedoce, A., Pimentel, D.R., Luptak, I., Adachi, T., Ido, Y., et al. (2019). Production of adeno-associated virus vectors for in vitro and in vivo applications. Sci. Rep. *9*, 13601. https://doi.org/10.1038/s41598-019-49624-w.
27. Zhao, H., Lee, K.-J., Daris, M., Lin, Y., Wolfe, T., Sheng, J., Plewa, C., Wang, S., and Meisen, W.H. (2020). Creation of a High-Yield AAV Vector Production Platform in Suspension Cells Using a Design-of-Experiment Approach. Mol. Ther. Methods Clin. Dev. *18*, 312–320. https://doi.org/10.1016/j.omtm.2020.06.004.
28. Dong, Y., Tran, A., Lee, J.-H., Garrett, G., Yang, J., Burke, D., Hsu, F., Fitch, R.J., Chang, D., and Jiang, M.-S. (2022). HEK293 Suspension Single Clonal Cell Line Readiness for High Productivity of Viral Vector Manufacturing. Mol. Ther. *30*, 192.
29. Jalšić, L., Lytvyn, V., Elahi, S.M., Hrapovic, S., Nassoury, N., Chahal, P.S., Gaillet, B., and Gilbert, R. (2023). Inducible HEK293 AAV packaging cell lines expressing Rep proteins. Mol. Ther. Methods Clin. Dev. *30*, 259–275. https://doi.org/10.1016/j.omtm.2023.07.002.

30. Lee, Z., Lu, M., Irfanullah, E., Soukup, M., and Hu, W.-S. (2022). Construction of an rAAV Producer Cell Line through Synthetic Biology. ACS Synth. Biol. *11*, 3285–3295. https://doi.org/10.1021/acssynbio.2c00207.

31. Su, W., Patrício, M.I., Duffy, M.R., Krakowiak, J.M., Seymour, L.W., and Cawood, R. (2022). Self-attenuating adenovirus enables production of recombinant adeno-associated virus for high manufacturing yield without contamination. Nat. Commun. *13*, 1182. https://doi.org/10.1038/s41467-022-28738-2.

32. Scarrott, J.M., Johari, Y.B., Pohle, T.H., Liu, P., Mayer, A., and James, D.C. (2023). Increased recombinant adeno-associated virus production by HEK293 cells using small molecule chemical additives. Biotechnol. J. *18*, 2200450. https://doi.org/10.1002/biot.202200450.

33. Khan, N., Cheemadan, S., Saxena, H., Bammidi, S., and Jayandharan, G.R. (2020). MicroRNA-based recombinant AAV vector assembly improves efficiency of suicide gene transfer in a murine model of lymphoma. Cancer Med. *9*, 3188–3201. https://doi.org/10.1002/cam4.2935.

34. Barnes, C.R., Lee, H., Ojala, D.S., Lewis, K.K., Limsirichai, P., and Schaffer, D.V. (2021). Genome-wide activation screens to increase adeno-associated virus production. Mol. Ther. Nucleic Acids *26*, 94–103. https://doi.org/10.1016/j.omtn.2021.06.026.

35. O'Driscoll, E.E., Arora, S., Lang, J.F., Davidson, B.L., and Shalem, O. (2024). CRISPR screen for rAAV production implicates genes associated with infection. Preprint at bioRxiv. https://doi.org/10.1101/2024.09.17.613356.

36. Reid, C.A., Grafton, F., Leveque-Eichhorn, L., Brim, J., Ukani, I., Fisher, K., and Mandegar, M.A. (2023). ATLAS: A High-Throughput Gain and Loss-of-Function Screening Platform for Optimizing AAV Production (ASGCT abstract 1616). Mol. Ther. *31*.

37. Ellis, B.L., Hirsch, M.L., Barker, J.C., Connelly, J.P., Steininger, R.J., and Porteus, M.H. (2013). A survey of ex vivo/in vitro transduction efficiency of mammalian primary cells and cell lines with Nine natural adeno-associated virus (AAV1-9) and one engineered adeno-associated virus serotype. Virol. J. *10*, 74. https://doi.org/10.1186/1743-422X-10-74.

38. Macůrek, L., Lindqvist, A., Lim, D., Lampson, M.A., Klompmaker, R., Freire, R., Clouin, C., Taylor, S.S., Yaffe, M.B., and Medema, R.H. (2008). Polo-like kinase-1 is activated by aurora A to promote checkpoint recovery. Nature *455*, 119–123. https://doi.org/10.1038/nature07185.

39. Archambault, V., and Carmena, M. (2012). Polo-like kinase-activating kinases. Cell Cycle *11*, 1490–1495. https://doi.org/10.4161/cc.19724.

40. Seki, A., Coppinger, J.A., Jang, C.-Y., Yates, J.R., and Fang, G. (2008). Bora and the Kinase Aurora A Cooperatively Activate the Kinase Plk1 and Control Mitotic Entry. Science *320*, 1655–1658. https://doi.org/10.1126/science.1157425.

41. De Luca, M., Lavia, P., and Guarguaglini, G. (2006). A functional interplay between Aurora-A, Plk1 and TPX2 at spindle poles: Plk1 controls centrosomal localization of Aurora-A and TPX2 spindle association. Cell Cycle *5*, 296–303. https://doi.org/10.4161/cc.5.3.2392.

42. Zitouni, S., Nabais, C., Jana, S.C., Guerrero, A., and Bettencourt-Dias, M. (2014). Polo-like kinases: structural variations lead to multiple functions. Nat. Rev. Mol. Cell Biol. *15*, 433–452. https://doi.org/10.1038/nrm3819.

43. Takagi, M., Honmura, T., Watanabe, S., Yamaguchi, R., Nogawa, M., Nishimura, I., Katoh, F., Matsuda, M., and Hidaka, H. (2003). In vivo antitumor activity of a novel sulfonamide, HMN-214, against human tumor xenografts in mice and the spectrum of cytotoxicity of its active metabolite, HMN-176. Invest. N. Drugs *21*, 387–399. https://doi.org/10.1023/a:1026282716250.

44. Gumireddy, K., Reddy, M.V.R., Cosenza, S.C., Boominathan, R., Baker, S.J., Papathi, N., Jiang, J., Holland, J., and Reddy, E.P. (2005). ON01910, a non-ATP-competitive small molecule inhibitor of Plk1, is a potent anticancer agent. Cancer Cell *7*, 275–286. https://doi.org/10.1016/j.ccr.2005.02.009.

45. Hörer, M., Sonntag, F., and Kober, R. (2019). Plasmid system. EP3722434B1. https://patents.google.com/patent/EP3722434B1/de.

46. Grafton, F., Feitzinger, R., Fisher, K., Leveque-Eichhorn, L., Reid, C.A., and Mandegar, M.A. (2023). Targeted CRISPR/Cas9 Screen Identifies Superior HEK293 Cell Lines for AAV9 Production. Mol. Ther. *31*.

47. Lens, S.M.A., Voest, E.E., and Medema, R.H. (2010). Shared and separate functions of polo-like kinases and aurora kinases in cancer. Nat. Rev. Cancer *10*, 825–841. https://doi.org/10.1038/nrc2964.

48. Milacic, M., Beavers, D., Conley, P., Gong, C., Gillespie, M., Griss, J., Haw, R., Jassal, B., Matthews, L., May, B., et al. (2024). The Reactome Pathway Knowledgebase 2024. Nucleic Acids Res. *52*, D672–D678. https://doi.org/10.1093/nar/gkad1025.

49. Gheghiani, L., Loew, D., Lombard, B., Mansfeld, J., and Gavet, O. (2017). PLK1 Activation in Late G2 Sets Up Commitment to Mitosis. Cell Rep. *19*, 2060–2073. https://doi.org/10.1016/j.celrep.2017.05.031.

50. Fu, Z., Malureanu, L., Huang, J., Wang, W., Li, H., van Deursen, J.M., Tindall, D.J., and Chen, J. (2008). Plk1-dependent phosphorylation of FoxM1 regulates a transcriptional programme required for mitotic progression. Nat. Cell Biol. *10*, 1076–1082. https://doi.org/10.1038/ncb1767.

51. Yu, F., He, H., Nastoupil, L.J., Xu-Monette, Z.Y., Pham, K., Liang, Y., Chen, G., Fowler, N.H., Yin, C.C., Tan, D., et al. (2022). Targetable vulnerability of deregulated FOXM1/PLK1 signaling axis in diffuse large B cell lymphoma. Am. J. Cancer Res. *12*, 4666–4679.

52. Otto, T., and Sicinski, P. (2017). Cell cycle proteins as promising targets in cancer therapy. Nat. Rev. Cancer *17*, 93–115. https://doi.org/10.1038/nrc.2016.138.

53. ClinicalTrials.gov (2024). https://clinicaltrials.gov/.

54. van Vugt, M.A.T.M., Gardino, A.K., Linding, R., Ostheimer, G.J., Reinhardt, H.C., Ong, S.-E., Tan, C.S., Miao, H., Keezer, S.M., Li, J., et al. (2010). A Mitotic Phosphorylation Feedback Network Connects Cdk1, Plk1, 53BP1, and Chk2 to Inactivate the G2/M DNA Damage Checkpoint. PLoS Biol. *8*, e1000287. https://doi.org/10.1371/journal.pbio.1000287.

55. Johnson, J.L., Yaron, T.M., Huntsman, E.M., Kerelsky, A., Song, J., Regev, A., Lin, T.-Y., Liberatore, K., Cizin, D.M., Cohen, B.M., et al. (2023). An atlas of substrate specificities for the human serine/threonine kinome. Nature *613*, 759–766. https://doi.org/10.1038/s41586-022-05575-3.

56. Wada, R. (2022). Enhancement of rAAV Productivity Utilizing HDAC Inhibitors on Helper-Free HEK293 Suspension Cell Culture Process. Mol. Ther. *30*.

57. Chung, C.-H., Murphy, C.M., Wingate, V.P., Pavlicek, J.W., Nakashima, R., Wei, W., McCarty, D., Rabinowitz, J., and Barton, E. (2023). Production of rAAV By Plasmid Transfection Induces Antiviral and Inflammatory Responses in Suspension HEK293 Cells. Mol. Ther. Methods Clin. Dev. *28*, 272–283. https://doi.org/10.1016/j.omtm.2023.01.002.

58. Wang, Y., Fu, Q., Lee, Y.S., Sha, S., and Yoon, S. (2023). Transcriptomic features reveal molecular signatures associated with recombinant adeno-associated virus production in HEK293 cells. Biotechnol. Prog. *39*, e3346. https://doi.org/10.1002/btpr.3346.

59. Pistek, M., Kahlig, C.-I., Hackl, M., Unterthurner, S., Kraus, B., Grabherr, R., Grillari, J., and Hernandez Bort, J.A. (2023). Comprehensive mRNA-sequencing-based characterization of three HEK-293 cell lines during an rAAV production process for gene therapy applications. Biotechnol. J. *18*, 2200513. https://doi.org/10.1002/biot.202200513.

60. Tworig, J., Grafton, F., Fisher, K., Hörer, M., Reid, C.A., and Mandegar, M.A. (2024). Transcriptomics-informed pharmacology identifies epigenetic and cell cycle regulators that enhance AAV production. Mol. Ther. Methods Clin. Dev. *32*, 101384. https://doi.org/10.1016/j.omtm.2024.101384.

61. Yu, Z., Deng, P., Chen, Y., Liu, S., Chen, J., Yang, Z., Chen, J., Fan, X., Wang, P., Cai, Z., et al. (2021). Inhibition of the PLK1-Coupled Cell Cycle Machinery Overcomes Resistance to Oxaliplatin in Colorectal Cancer. Adv. Sci. *8*, 2100759. https://doi.org/10.1002/advs.202100759.

62. Smith, L., Farzan, R., Ali, S., Buluwela, L., Saurin, A.T., and Meek, D.W. (2017). The responses of cancer cells to PLK1 inhibitors reveal a novel protective role for p53 in maintaining centrosome separation. Sci. Rep. *7*, 16115. https://doi.org/10.1038/s41598-017-16394-2.

63. Normandin, K., Coulombe-Huntington, J., St-Denis, C., Bernard, A., Bourouh, M., Bertomeu, T., Tyers, M., and Archambault, V. (2023). Genetic enhancers of partial PLK1 inhibition reveal hypersensitivity to kinetochore perturbations. PLoS Genet. *19*, e1010903. https://doi.org/10.1371/journal.pgen.1010903.

64. Maddalena, A., Dell'Aquila, F., Giovannelli, P., Tiberi, P., Wanderlingh, L.G., Montefusco, S., Tornabene, P., Iodice, C., Visconte, F., Carissimo, A., et al. (2018). High-Throughput Screening Identifies Kinase Inhibitors That Increase Dual Adeno-Associated Viral Vector Transduction *In Vitro* and in Mouse Retina. Hum. Gene Ther. *29*, 886–901. https://doi.org/10.1089/hum.2017.220.

65. Sakaue-Sawano, A., Kurokawa, H., Morimura, T., Hanyu, A., Hama, H., Osawa, H., Kashiwagi, S., Fukami, K., Miyata, T., Miyoshi, H., et al. (2008). Visualizing Spatiotemporal Dynamics of Multicellular Cell-Cycle Progression. Cell *132*, 487–498. https://doi.org/10.1016/j.cell.2007.12.033.

66. Andrews, S. (2010). FastQC: A Quality Control Tool for High Throughput Sequence Data http://www.bioinformatics.babraham.ac.uk/projects/fastqc/.

67. Bolger, A.M., Lohse, M., and Usadel, B. (2014). Trimmomatic: a flexible trimmer for Illumina sequence data. Bioinformatics *30*, 2114–2120. https://doi.org/10.1093/bioinformatics/btu170.

68. Kim, D., Paggi, J.M., Park, C., Bennett, C., and Salzberg, S.L. (2019). Graph-based genome alignment and genotyping with HISAT2 and HISAT-genotype. Nat. Biotechnol. *37*, 907–915. https://doi.org/10.1038/s41587-019-0201-4.

69. Liao, Y., Smyth, G.K., and Shi, W. (2014). featureCounts: an efficient general purpose program for assigning sequence reads to genomic features. Bioinformatics *30*, 923–930. https://doi.org/10.1093/bioinformatics/btt656.

70. Akhmedov, M., Martinelli, A., Geiger, R., and Kwee, I. (2020). Omics Playground: a comprehensive self-service platform for visualization, analytics and exploration of Big Omics Data. NAR Genom. Bioinform. *2*, lqz019. https://doi.org/10.1093/nargab/lqz019.

71. Agrawal, A., Balcı, H., Hanspers, K., Coort, S.L., Martens, M., Slenter, D.N., Ehrhart, F., Digles, D., Waagmeester, A., Wassink, I., et al. (2024). WikiPathways 2024: next generation pathway database. Nucleic Acids Res. *52*, D679–D689. https://doi.org/10.1093/nar/gkad960.

72. Szklarczyk, D., Gable, A.L., Nastou, K.C., Lyon, D., Kirsch, R., Pyysalo, S., Doncheva, N.T., Legeay, M., Fang, T., Bork, P., et al. (2021). The STRING database in 2021: customizable protein-protein networks, and functional characterization of user-uploaded gene/measurement sets. Nucleic Acids Res. *49*, D605–D612. https://doi.org/10.1093/nar/gkaa1074.